A Numerical Study of the Transverse Modulus of Wood as a Function of Grain Orientation and Properties

By J. A. Nairn[1]
Wood Science & Engineering, Oregon State University, Corvallis, OR 97331, USA

Keywords

Finite element analysis
Grain Orientation
Numerical modeling
Shear Coupling
Transverse modulus

Summary

Finite element analysis was used to study the effective transverse modulus of solid wood for all possible end-grain patterns. The calculations accounted for cylindrical anisotropy of wood within rectangular specimens and explicitly modeled wood as a composite of earlywood and latewood. The effective modulus was significantly reduced by growth ring curvature or off-axis loading, The large changes were attributed to the low transverse shear modulus of wood. The explicit, or heterogeneous, model was compared to prior numerical methods that homogenized properties in the transverse plane. The two models gave similar effective modulus results, but a heterogeneous model was required to capture details in modulus calculations or to realistically model stress concentrations. Various numerical methods for modeling transverse stresses in wood are discussed

Introduction

Wood within a tree has cylindrical symmetry. Its longitudinal direction is along the tree's axis while the radial and tangential directions are in the transverse plane. A transverse cross section of a tree has approximately concentric growth rings. The radial and tangential directions are perpendicular and parallel to these rings. Typical boards are sawn from trees with rectangular cross sections. A board's axial direction aligns with the tree's longitudinal direction, but its cross section will have various end-grain patterns depending on where it was cut from the tree (see Fig. 1). The various board cross sections are a consequence of fitting a material with cylindrical symmetry into a shape with rectangular symmetry. This paper describes a numerical study of the transverse properties and stresses for rectangular boards as a function of the end grain pattern.

Because the longitudinal modulus (E_L) of wood is 10 to 20 times larger than the radial or tangential modulus (E_R or E_T), while E_R and E_T are similar, one is tempted to approximate wood as transversely isotropic. But, in reality, E_R is typically double E_T (Bodig 1982); this difference should not be ignored for accurate modeling of transverse stresses. In hardwoods, the stiffer radial direction may be due to rays cells (Price 1929;

Schniewind 1959). In softwoods, the stiffer radial direction may be due to alignment of cells in radial rows (Price 1929). Whatever the reason, transverse anisotropy causes some unusual experimental results. Bodig (1963; 1965) observed that E_R of Douglas fir increases as specimen thickness increases. In contrast, Hoffmeyer *et al*. (2000) found that E_R of Norway spruce decreases as gage length increases. Kennedy (1968) measured transverse modulus as
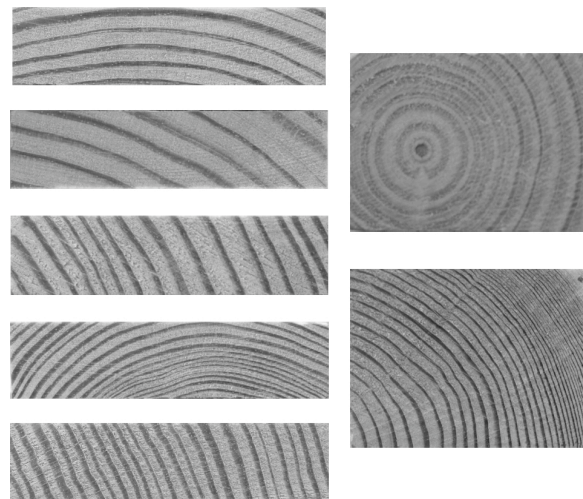

Fig. 1: Sample end grain patterns for rectangular boards cut from a tree with cylindrical structure.

---

a function of loading angle for several species and found that the modulus varies with angle and can even be lower than both E_R and E_T. Shipsha and Berglund (2006) found that E_R of periphery boards far from the pith of Norway spruce is more then double the E_R for boards close to the pith.

These observations are a consequence of the transverse anisotropy of wood and of fitting a cylindrical material into a rectangular specimen. They are also influenced by the particularly low transverse shear modulus, G_{RT}, of wood. A low G_{RT} combined with growth ring curvature causes localized deformations that affect modulus experiments (Aicher and Dill-Langer 1996, Aicher *et al*. 2001; Shipsha and Berglund 2006). Another wood property that may play a role, but is less studied, is the layering of wood into earlywood and latewood material within each growth ring; *i.e.*, the composite structure of solid wood.

A thorough understanding of transverse anisotropy and layering of wood is helpful for analysis of structures and transverse failure modes. For example, variations in end-grain patterns between boards in glulam cause modulus mismatches between layers. These mismatches can induce non-uniform stresses that may promote glue-line failure or transverse tensile failure (Aicher and Dill-Langer 1997; Hoffmeyer *et al*. 2000). Non-uniform stresses are particularly important for curved glulam subjected to climate changes (Aicher and Dill-Langer 1997; Aicher *et al*. 1998). Transverse stress analysis is also important for modeling drying cracks or internal checking of Radiata pine (Pang *et al*. 1999; Ball *et al*. 2001). Since internal checking is confined to earlywood, its analysis requires composite analysis of wood that explicitly accounts for earlywood and latewood properties.

Previous finite element analyses (FEA) of transverse wood properties confirm that transverse anisotropy and low shear modulus are important. Aicher and Dill-Langer (1996) did FEA of one wide, symmetric board under radial loading and various boundary conditions. Growth ring curvature within the board strongly affected the effective modulus. Hoffmeyer *et al*. (2000) did FEA of glulam with boards loaded in the radial direction and one selected timber structure under tangential loading. The stress concentrations correlated with observed transverse cracks. Aicher et al. (2001) compared experiments to FEA results

on a specific board under tangential loading. The experiments confirm the effect of low G_{RT} on transverse wood properties. Jernkvist and Thuvander (2001) used optical methods to measure radial dependence of mechanical properties. These properties were input to FEA analysis for radial loading of boards of various widths as a function of distance from the pith. Shipsha and Berglund (2006) compared FEA results to radial loading of a board close to the pith and one far from the pith to confirm shear coupling effects in modulus experiments.

Previous numerical studies mostly used homogenized properties in the transverse plane and analyzed only selected loadings or selected board orientations. The purposes of this paper were to explicitly model earlywood and latewood, to compare such heterogeneous calculations to calculations with homogenized transverse properties, and to sample many more end-grain patterns. Various numerical approaches to modeling transverse mechanical properties of wood are discussed.

Numerical Methods

Figure 2 shows one quadrant of an idealized tree with concentric growth rings of earlywood and latewood. All potential cross sections for rectangular lumber can be sampled from this quadrant by selecting board centroid, (x_c, y_c), while maintaining board width and height in the x and y directions. Boards selected this way were analyzed by 2D, plane-strain FEA. The FEA mesh was created by partitioning a board's entire cross section into a square grid of 8-noded, isoparametric elements. All elements used orthotropic material properties with the tangential, radial, and longitudinal properties initially in the x, y, and z directions. To account for cylindrical anisotropy of wood, each element's material axes were rotated clockwise by angle

$$\theta = \frac{\pi}{2} - \arctan \frac{y_c^{(i)}}{x_c^{(i)}} \qquad (1)$$

where $(x_c^{(i)}, y_c^{(i)})$ is the centroid of element *i*. To model heterogeneous properties, each element was assigned to either earlywood or latewood properties depending on radial position of the element centroid. Defining board orientation by centroid is equivalent to a prior approach based
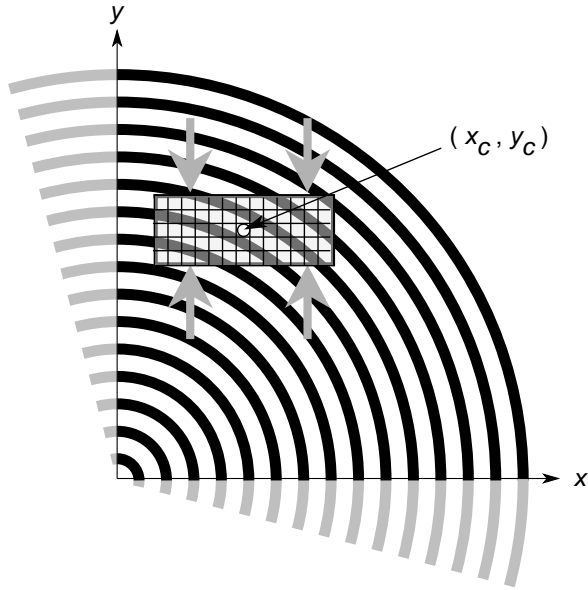
Fig. 2: All possible board orientations can be sampled by orienting the width and height direction along the *x* and *y* axes and selecting the board centroid, ($\underline{x}_c$, y_c), from the upper-right quadrant of the *x-y* plane. The inset board indicates the FEA mesh was a square grid of elements and loading was in the *y* direction.

on distance from board bottom to the pith, *d*, and eccentricity, *e*, or distance from board center to a vertical line from the pith (Aicher and Dill-Langer 1996; 1997). The two methods are related by $d = y_c - h/2$ and $e = x_c$, where *h* is board height.

The effective, plain-strain, transverse modulus was determined by subjecting each board to axial compression in the *y* direction. Loading was either by uniform displacement or uniform stress conditions. When a board is explicitly heterogeneous (*i.e.*, modeled with earlywood and latewood layers), the stress state is non-uniform and complex. The modulus was thus found by energy methods. For uniform displacement conditions, total strain energy, U_ε, can be expressed in terms of an effective modulus, E_ε^*, as (Hashin 1969)

$$U_\varepsilon = \frac{V}{2} E_\varepsilon^* \varepsilon^2 \tag{2}$$

where V is total volume. Thus, the effective modulus is given by

$$E_\varepsilon^* = \frac{2U_\varepsilon}{V\varepsilon^2} \tag{3}$$

Similarly, for uniform stress conditions

$$U_\sigma = V \frac{\sigma^2}{2E_\sigma^*} \quad \text{and} \quad E_\sigma^* = \frac{V\sigma^2}{2U_\sigma} \tag{4}$$

The two energies, U_ε and U_σ, are total strain energies found by FEA.

All simulations were for Douglas fir; typical bulk properties for the longitudinal (*L*), radial (*R*), and tangential (*T*) directions are listed in Table 1 (Bodig and Jayne 1982). To explicitly model earlywood and latewood, one needs their relative fractions and their separate properties. Growth ring thickness in Douglas fir varies from 2 to 11 mm, depending on location within the tree (larger closer to the pith) and on yearly variations in growing rates; the average value is 3.5 ± 2 mm (Taylor *et al.* 2003; Grotta *et al.* 2005). X-Ray densitometer measurements show an average latewood fraction of 40% (Abdel-Gadir, *et al.* 1993). All simulations matched these average properties by setting earlywood thickness to 2.1 mm and latewood thickness to 1.4 mm.

There are few experiments on mechanical properties of earlywood and latewood (Jernkvist and Thuvander 2001), but some qualitative information is available. The earlywood and latewood properties assumed for most calculations are listed in Table 1. These properties were derived as follows.:

Tangential Modulus: Cellular mechanics predicts that transverse moduli scale with the cube of the density (Gibson *et al.* 1982; Gibson and Ashby 1997). It was thus assumed that

$$E_T^{(l)} = E_T^{(e)} \rho^3 \tag{5}$$

where ρ is the ratio of latewood to earlywood density and superscripts (*l*) and (*e*) indicate latewood and earlywood properties.

Radial Modulus: This modulus is also a transverse modulus, but recent experiments show the the scaling is less than ρ^3 (Modén and Berglund, 2006). The reduced scaling is caused by alignment of cells in radial rows leading to axial deformations that are ignored in cellular theories. Here it was assumed that

$$E_R^{(l)} = E_R^{(e)} \rho^{1.63} \tag{6}$$

where 1.63 was an arbitrary scaling coefficient between 1 and 3.

Values for Transverse Moduli: The above transverse moduli ratios were used in FEA calculations for pure radial loading ($x_c = 0$ and

Table 1: Cylindrically orthotropic material properties for bulk wood, earlywood, and latewood used in the calculations to model Douglas fir in the longitudinal (L), radial (R), and tangential (T) directions. No properties are listed for longitudinal shear moduli (G_{LR} and G_{LT}) because they have no effect on 2D, plain-strain analyses.

Property	Bulk	Earlywood	Latewood
E_T (MPa)	620	152	1215
E_R (MPa)	960	566	1752
E_L (MPa)	14500	10400	20700
G_{RT} (MPa)	80	50	215
ν_{TR}	0.35	0.30	0.425
ν_{TL}	0.033	0.033	0.033
ν_{RL}	0.041	0.041	0.041
fraction	—	0.60	0.40

y_c large) and pure tangential loading ($y_c = 0$ and x_c large) and varied until the effective moduli agreed with bulk values for E_R and E_T. The density ratio for Douglas fir was set to $\rho = 2$ (Abdel-Gadir, *et al*. 1993). The resulting moduli are given in Table 1.

Transverse Shear Modulus: This modulus was found by selecting a reasonable value $G_{RT}^{(e)}$ and then varying $G_{RT}^{(l)}$ until FEA calculations matched the bulk shear modulus. Pure shear FEA conditions were set by fixing the entire boundary to a pure shear deformation state. A
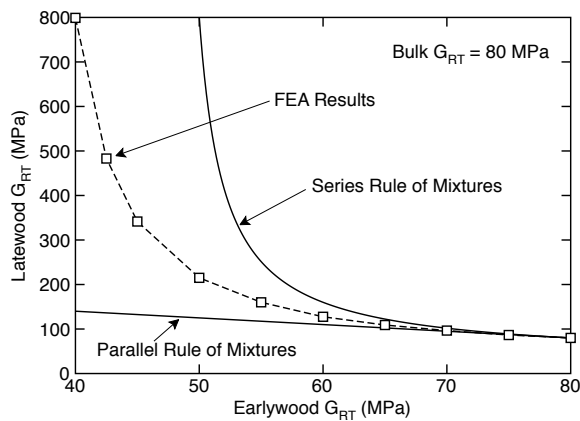

Fig. 3: Latewood shear modulus as a function of earlywood shear modulus when the bulk shear modulus is equal to 80 MPa. The solid lines are calculations of latewood shear modulus using simple composite theories based on springs in parallel or in series.

plot of $G_{RT}^{(l)}$ as a function of $G_{RT}^{(e)}$ is given in Fig. 3. The results are bounded by a simple rule of mixtures (parallel springs) and an inverse rule of mixtures (series springs), but trends closer to the later, as often assumed in composite mechanics for shear modulus (Jones 1975). Unless specified, all calculations assumed the specific shear moduli listed in Table 1.

Transverse Poisson Ratio: Optical measurements show that $\nu_{TR}^{(l)} > \nu_{TR}^{(e)}$ (Jernkvist and Thuvander 2001). The values in Table 1 were selected consistent with this finding and such that a rule of mixtures gave the bulk Poisson ratio:

$$\nu_{TR} = 0.35 = V_e \nu_{TR}^{(e)} + V_l \nu_{TR}^{(l)} \qquad (7)$$

where $V_e = 0.6$ is the fraction earlywood and $V_l = 0.4$ is the fraction latewood.

Longitudinal Modulus: Cellular mechanics predicts that longitudinal modulus scales linearly with density (Gibson and Ashby 1997). The values in Table 1 were selected to follow this scaling and such that a rule of mixtures gave the bulk longitudinal modulus:

$$E_L = 14,500 = V_e E_L^{(e)} + V_l E_L^{(l)} \qquad (8)$$

Longitudinal Poisson Ratios: The longitudinal modulus and Poisson ratios enter plane-strain calculations through plane-strain modifications to the in-plane moduli. For example, the *effective*, plain-strain radial modulus is

$$\frac{1}{E_R^{(eff)}} = \frac{1}{E_R} - \frac{E_L \nu_{RL}^2}{E_R^2} \qquad (9)$$

Since longitudinal properties only have a small effect, the Poisson ratios simply used the bulk Poisson ratios for both earlywood and latewood.

Other Poisson Ratios: Poisson ratios not listed obeyed the relation

$$\nu_{ji} = \frac{E_j \nu_{ij}}{E_i} \qquad (10)$$

In summary, the earlywood and latewood properties in Table 1 are not experimental results. They are, however, reasonable values, consistent with known theory and experiments on earlywood and latewood properties, and consistent with bulk properties.

All calculations were run using the author's FEA software (Nairn 2006). FEA Convergence for effective modulus was checked by varying the uniform grid size from 2X2 mm down to 0.25X0.25 mm elements. These calculations found effective modulus for 10 different board orientations. Element sizes 0.5X0.5 mm and smaller gave nearly identical results, while larger elements had minor differences. All subsequent calculations thus used 0.5X0.5 mm elements.

Using a square grid to model curved growth rings can result in rough boundaries between earlywood and latewood, although the roughness is small for fine meshes. To check for numerical problems caused by rough boundaries, some calculations used a modified grid where nodes near earlywood-latewood boundaries were moved to those boundaries. The differences between a square grid and a modified grid for modulus calculations were negligible. A drawback of the modified grid is that node movement sometimes distorted elements causing unrealistic strain calculations. All calculations therefore used the simpler square grid.

Results and Discussion

Modulus as a function of board orientation

To probe all board orientations, the quadrant in Fig. 2 was partitioned into a grid extending from 0 to 500 mm in each direction with grid points separated by 25 mm. FEA calculations were run for 50X20 mm boards located at each of the 441 grid points. Each FEA calculation used a 0.5X0.5
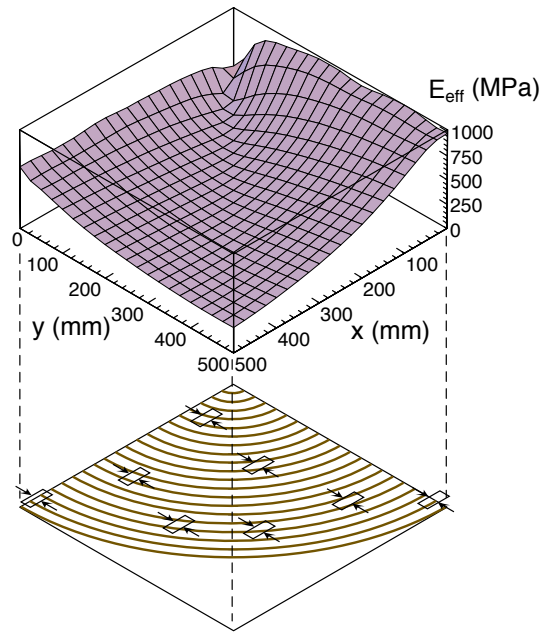

Fig. 4: The effective transverse modulus as a function of board centroid for all possible board orientations. The loading was in the y direction. The boundary conditions were uniform axial displacement.

mm square grid resulting in 4000 elements with 12281 nodes to mesh the entire board. The effective modulus as a function of position, calculated using uniform displacement conditions, is plotted in Fig. 3. For radial loading ($x_c = 0$), the modulus was low near the pith, but increased as y_c increased. Far from the pith ($x_c = 0$, y_c large), the modulus approached the bulk E_R. The radial loading results are analogous to numerical results by Jernkvist and Thuvander (2001) and experimental and numerical results by Shipsha and Berglund (2006). Pure tangential loading ($y_c = 0$) was similar, except with a smaller increase because the bulk E_T is smaller. For orientations deviating from pure radial or tangential loading, the modulus rapidly decreased. The rapid decrease is a consequence of the low transverse shear modulus (Aicher and Dill-Langer 1996; Aicher et al. 2001; Shipsha and Berglund 2006). A shear effect maximizes near 45° where a wide trough of minimum stiffness was observed. Common practice for measuring transverse properties of wood is to select small, straight-grained specimens and measure bulk E_R and E_T (ASTM D-143 2001). From the FEA grid results, however, the effective transverse modulus was
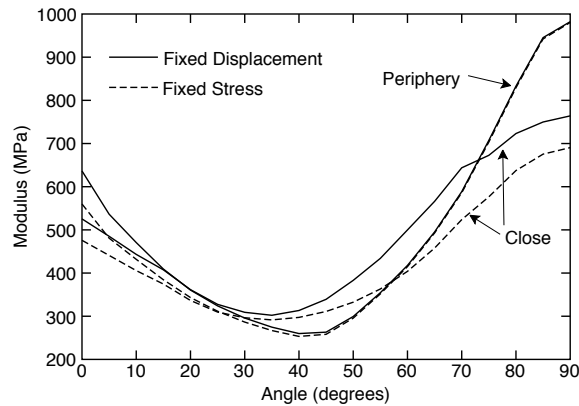
Fig. 5: The effective modulus as a function of angle for "Close" boards (centroid 50 mm from the pith) and "Periphery" boards (centroid 500 mm from the pith). The solid lines used uniform displacement boundary conditions while the dashed lines used uniform stress boundary conditions.

lower than both E_R and E_T for 82% of the orientations.

The grid calculations were repeated for uniform stress instead of uniform displacement conditions. Figure 5 plots the effective modulus for boards at two constant distances from the pith as a function of angle between a line to the board centroid and the x axis. "Close" boards were 50 mm from the pith while "Periphery" boards where 500 mm from the pith. The moduli by uniform stress or uniform displacement conditions were similar, although the uniform displacement result was always stiffer. By variational mechanics, a modulus found by imposing displacement boundary conditions and minimizing potential energy (*i.e.*, the FEA process) is a rigorous upper bound to the modulus (Hashin 1969). Although the uniform stress result is not a lower bound (because that would require minimization of complementary energy), it must be lower than the upper-bound. Because the FEA analysis is converged, however, both results should be accurate. All subsequent calculations used uniform displacement conditions.

Heterogeneous calculations vs. homogenized calculations

To study whether layering influences properties, calculations explicitly modeling earlywood and latewood were compared to calculations using homogenized properties (see Bulk properties in Table 1). Although all elements had the same

material properties, each element was still assigned the appropriate angle to model a cylindrically anisotropic material. The modulus for periphery and close boards calculated with homogenized properties (dashed lines) is compared to the heterogeneous model (solid lines) in Fig. 6. The similarities show that a homogenized model provided an acceptable approximation for modulus. Differences, however, did arise. For example, the modulus for close boards at low angle was more than 20% stiffer when using homogenized properties. Similarly, the modulus for periphery boards around 15° was more than 15% stiffer with homogenized properties.

Another method to compare homogenized and heterogeneous models is to vary the earlywood and latewood properties while keeping bulk properties constant. If layering plays a role in mechanical properties, heterogeneous calculations would vary while homogenized calculations would be constant. Figure 7 shows the modulus of periphery boards for homogenized properties (dashed line) and for heterogeneous calculations with three combinations of shear moduli for earlywood and latewood. The earlywood modulus was set to 40 MPa, 50 MPa, or 80 MPa while the latewood modulus was selected to keep the bulk transverse shear modulus equal to 80 MPa. The required latewood shear moduli (from Fig. 3) were 800 MPa, 215 MPa, and 80 MPa, respectively. All models gave the same results at 0°, near 45°, and at 90°, but for other angles,
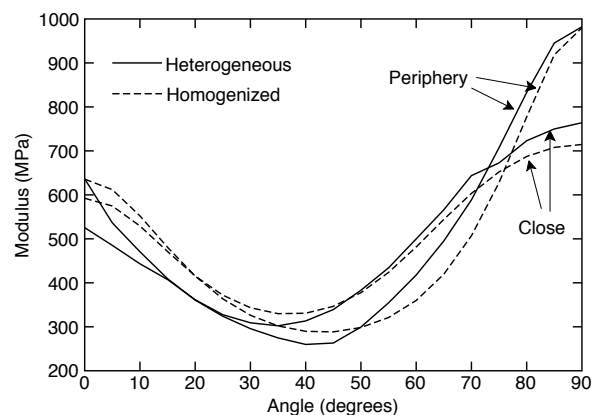

Fig. 6: The effective modulus as a function of angle for "Close" boards (centroid 50 mm from the pith) and "Periphery" boards (centroid 500 mm from the pith). The solid lines used a heterogeneous analysis that explicitly modeled earlywood and latewood while the dashed lines used homogenized transverse properties.
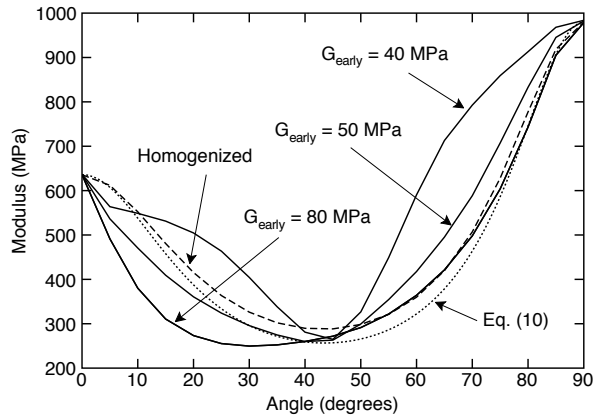
Fig. 7: The effective modulus as a function of angle for "Periphery" boards (centroid 500 mm from the pith). The solid lines used a heterogeneous analysis and varied earlywood and latewood shear modulus while keeping the bulk shear modulus constant at 80 MPa. The dashed line used homogenized properties in the transverse plane. The dotted line is the prediction for a rectangularly-orthotropic material given by Eq. (11).

layering influenced the results. The counterintuitive increase in modulus as earlywood shear modulus decreased was because the latewood shear modulus increased more than the earlywood shear modulus decreased. In brief, the layered structure of wood and the relative properties of the layers influence transverse stiffness. A heterogeneous model is required to capture these layering effects.

One approach to measuring the transverse shear modulus of anisotropic materials is do off-axis stress-strain experiments (Price 1929). If a material is rectilinearly anisotropic, rotation of the stiffness matrix gives modulus as a function of angle as (Jones 1975)

$$\frac{1}{E_\theta} = \frac{\cos^4\theta}{E_x} + \left(\frac{1}{G_{xy}} - \frac{2\nu_{xy}}{E_x}\right)\sin^2\theta\cos^2\theta + \frac{\sin^4\theta}{E_y} \quad (11)$$

This function is plotted in Fig. 7 (dotted line). The small differences between Eq. (11) and the homogenized analysis are due to slight growth ring curvature in periphery boards ignored in the equation, but included in the homogenized numerical results. If E_x and E_y are known, measurement of E_θ can be solved to find G_{xy}. Experiments are usually done at 45° where the shear effect is the largest and the test would be most sensitive for calculation of G_{xy}. The new heterogeneous model results (Fig. 7) show that 45° experiments are insensitive to the analysis and thus can measure bulk G_{RT}. For any other angle, however, the modulus depends on the relative shear moduli of earlywood and latewood. Perhaps this effect could be exploited to measure earlywood and latewood shear moduli. The suggested experiment is to measure transverse modulus as a function of angle. Results at 0°, 45°, and 90° would measure bulk E_T, G_{RT}, and E_R; results between those angles could be fit using a
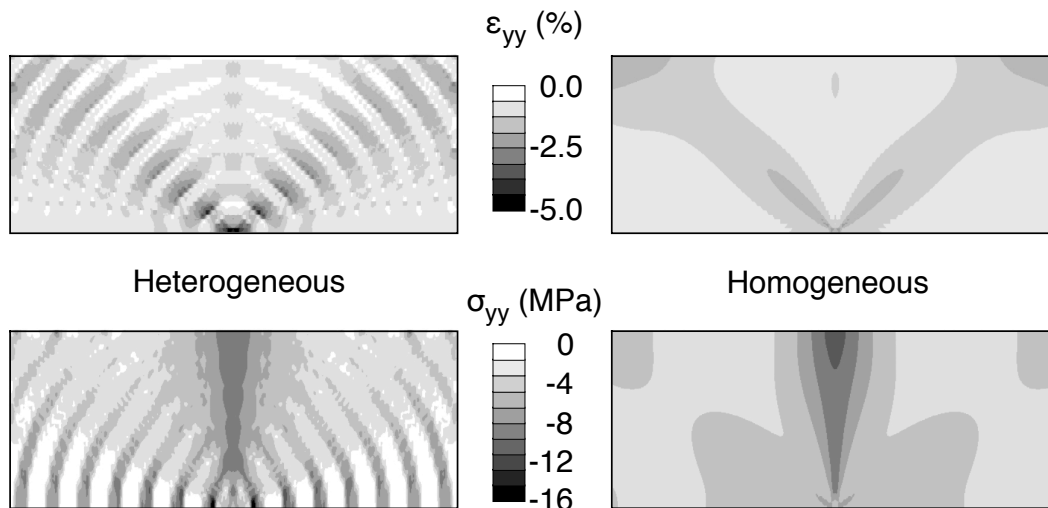

Fig. 8: Contours of *y*-direction normal strain and stress calculated by either a heterogeneous analysis or a homogeneous analysis. The applied strain was -1.0%. The average stresses were -4.14 MPa for the heterogeneous analysis and -4.40 MPe for the homogeneous analysis.

heterogeneous model to determine earlywood and latewood G_{RT}.

The differences between a heterogeneous and homogenized analysis are much larger for strain and stress distributions. Figure 8 has contour plots for strains and stresses in a 50✕20 mm board with centroid (0,10); *i.e.*, radial loading for a board with its lower edge at the center of the tree. For the homogenized model (right of Fig. 8), the patterns are similar to previous calculations (Shipsha and Berglund 2006). The applied strain was -1%, but the shear effect caused higher strains at 45˚; the maximum strain was -2.28%. The average stress was -4.40 MPa, but the maximum stress near the specimen center was -10.9 MPa. The underlying patterns in the heterogeneous model (left of Fig. 8) were similar, but the strains and stresses redistribute in earlywood and latewood due to their differing mechanical properties. The redistribution caused greater extremes. The maximum strains occurred in the lower-stiffness earlywood at 45˚ and reached -4.95%. While the average stress changed only slightly to -4.14 MPa, the maximum stresses occurred in the stiffer latewood at the bottom of the board and reached -15.4 MPa. Thus, when local stress concentrations are crucial to modeling, such as in failure modeling, a heterogeneous model is required to capture those values. A homogenized model may significantly underestimate stress concentrations.

Effect of board dimensions

Since the effective modulus depends on growth ring curvature across a board, the results depend on board dimensions. To assess dimension effects, calculations were run for 25.4 mm (1.0 in) wide boards with thickness varying from 25.4 mm to 76.2 mm (1.0 in to 3.0 in). These boards were narrower and thicker than in previous calculations. The radial loading results ($x_c = 0$) as a function of distance from the pith (y_c) are given in Fig. 9. For comparison, the previous results for 50✕20 mm boards are also plotted (dotted line). Each FEA calculation used a 0.5✕0.5 mm square grid and uniform displacement boundary conditions.

Like previous results, the effective modulus for radial loading of narrower boards was lower when near the pith, but increased to the bulk radial modulus for periphery boards. Compared to wider boards, the transition to bulk modulus was faster
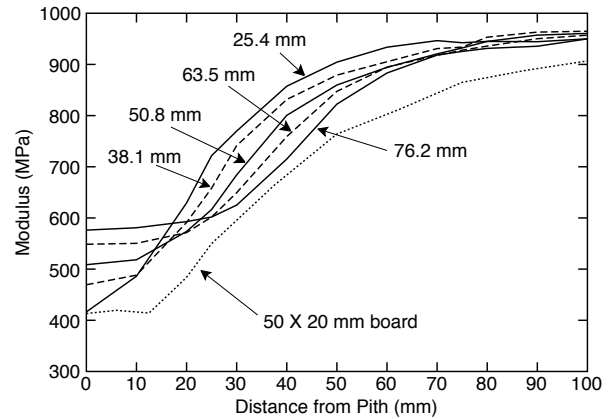

Fig. 9: The effective modulus as a function of distance of the pith for radial loading. The solid and dashed curves are the results for a board of width 25.4 mm and various thicknesses. The dotted line compares to previous results for a 50✕20 mm board.

because the edges of narrower boards had less growth ring curvature. These results are similar to previous numerical results for radial loading as a function of width by Jernkvist and Thuvander (2001). As the board got thicker, the difference between pith boards and periphery boards got smaller. For boards near the pith (*e.g.*, $y_c = 0$), increased thickness includes extra periphery material and thus the effective modulus increased. For boards in the middle (e.g., $y_c = 40$ mm), increased thickness includes extra pith material and thus the effective stiffness decreased. For periphery boards, growth ring curvature eventually becomes negligible and the effective modulus approached the bulk radial modulus.

The board dimensions were selected to match experiments on Douglas fir by Bodig (1963, 1965), where the radial modulus doubled as the thickness increased from 25.4 mm (1.0 in) to 76.2 mm (3.0 in). Unfortunately, Bodig did not specify the distance of the boards from the pith. Although impossible to quantitatively model the experiments, the results in Fig. 9 show that a doubling of modulus is possible depending on board selection. Bodig's (1965) second paper claims the boards were selected with constant y_c, although it also gave no value for y_c. Such constant y_c experiments can be predicted by intersections of a vertical line through y_c with the curves for different thicknesses. Thus, if y_c was 0, the modulus would increase with thickness by

38%, But, if y_c was 40 mm, the modulus would decrease by 17%. This latter prediction disagrees with Bodig's results (1962, 1965), but agrees with more recent results for modulus as a function of gage-length by Hoffmeyer *et al*. (2000).

Approaches to numerical modeling

Four common methods for numerical modeling of wood are discussed with emphasis on their suitability for problems involving stress analysis in the transverse plane:

1. **Transversely Isotropic Material**: The simplest model of wood assumes it is transversely isotropic with the axial direction in the longitudinal direction. The rational is that longitudinal modulus is 10-20 times larger than radial or tangential moduli, while those transverse moduli may differ by less than a factor of two. Approximating transverse properties as isotropic, even if the radial and tangential moduli were identical, is a serious error because it does not allow a low transverse shear modulus, G_{RT}, which is important to transverse properties. In an isotropic plane, the shear modulus is typically one-third the tensile moduli (depending on Poisson's ratio), but in wood, G_{RT} is 10-20 times smaller than the transverse moduli.

2. **Rectilinear Orthotropic Material**: This model accounts for wood being orthotropic, but simplifies the analysis by aligning coordinates of the anisotropy with the rectilinear global axes, *i.e.*, tangential, radial, and longitudinal directions in x, y, and z directions or at a constant angle to those directions. This approach simplifies finite element analysis because all elements have the same orientation for their material axes. Because this model can include low shear moduli, it can account for changes in effective modulus due to off-axis loading. The rectilinear assumption, however, makes it only suitable for boards far from the pith. It would completely miss board dimension and orientation effects caused by growth ring curvature within a specimen.

3. **Homogenized Cylindrical Orthotropy**: This model accounts for growth ring curvature within a specimen, but simplifies the analysis by using homogenized properties in the transverse plane. Compared to rectilinear orthotropy, cylindrical orthotropy complicates the mesh generation. In rectilinear orthotropy, one can use larger elements where stress gradients are small, but in cylindrical orthotropy, small elements are required throughout the specimen in order to resolve orientation of material axes along curved growth rings. An homogenized analysis can approximate effective mechanical properties, account for differences between pith and periphery boards, and account for size effects.

4. **Heterogeneous Cylindrical Orthotropy**: The model used here accounts for both growth ring curvature within a specimen and variations in material properties between earlywood and latewood. This model is physically the closest to approximating the structure of real wood. Although a fine mesh is required to resolve the structure of wood, the extra effort versus homogenized cylindrical orthotropy is minimal. Since the homogenized approach needs a fine mesh to resolve material angle, the only extra work is to additionally assign each element to either earlywood or latewood properties. If earlywood and latewood are particularly thin, the heterogeneous analysis would require an even finer mesh and thus could be more complicated. Differences between homogenized and heterogeneous analyses were discussed above. The most significant differences were the stress concentrations caused by stress and strain partitioning between earlywood and latewood. A heterogeneous analysis is recommended for modeling failure processes induced by localized stresses. The main problem with explicitly modeling earlywood and latewood is having reliable values for their mechanical properties. This paper used reasonable properties. New experimental work to measure their properties would be beneficial.

Conclusions

Numerical modeling of solid wood under transverse loading was done for all possible end grain patterns within rectangular specimens. The effective modulus was strongly affected by loading direction. It was particularly low when the loading direction was neither radial nor tangential over some parts of the board. This off-axis loading effect was due to wood's low transverse shear modulus. Calculations explicitly modeling earlywood and latewood were

compared to calculations using homogenized transverse-plane properties. The results were qualitatively similar for effective modulus, but significantly different for stress concentrations. Modeling all effects of transverse stresses, particularly when cracking or failure properties are involved, thus requires explicit modeling of the layered structure of wood. Such calculations need more reliable information for the mechanical properties of earlywood and latewood..

Acknowledgements

References

Abdel-Gadir, A. Y., Krahmer, R. L., McKimmy, M. D. (1993) Intra-ring variations in mature Douglas-fir trees from Provenance plantations. *Wood and FIber Science,* 25(2):170–181.

Aicher, S., Dill-Langer, D. (1996) Influence of cylindrical anisotropy of wood and loading conditions on off-axis stiffness and stresses of a board in tension perpendicular to the grain. *Otto Graf Journal*, 7:216–242.

Aicher S., Dill-Langer, G. (1997) Climate induced stresses perpendicular to the grain in glulam. *Otto Graf Journal*, 8:209–231.

Aicher, S., Dill-Langer, G., Ranta-Maunus, A. (1998) Duration of load effect in tension perpendicular to the grain of glulam in different climates. *Holz Roh- Werkstoff*, 56(5):295–205.

Aicher, S., Dill-Langer, G., Hofflin, L. (2001) Effect of polar anisotropy of wood loaded perpendicular to grain. *Journal of Materials in Civil Engineering*, 13(1):2–9.

ASTM D-143 (2001) Standard test methods for small clear specimens of timber. *Annual Book of ASTM Standards*, Volume 4.10 Wood, 25–55.

Ball, R. D. , McConchie, M., and Cown, D. J. (2001) Heritability of internal checking in Pinus Radiata — Evidence and preliminary estimates. *New Zealand Journal of Forestry Science*, 31(1):78–87.

Bodig, J. (1963) The peculiarity of compression of conifers in radial direction. *Forest Products J.*, 13:438.

Bodig, J. (1965) The effect of anatomy on the initial stress-strain relationship in transverse compression. *Forest Products J.*, 15:197–202.

Bodig, J., Jayne, B. A. (1982) Mechanics of Wood and Wood Composites. Van Nostran-Reinhold Co, Inc., New York.

Gibson, L. J., Ashby, M. F., Schajer, G. S., Robertson, C. I. (1982) The mechanics of two-dimensional cellular materials. *Proc. Royal Soc. Lond. A,* 382:25–42.

Gibson, L. J., Ashby, M. F. (1997) Cellular Solids: Structure and Properties. Cambridge University Press, Cambridge, England.

Grotta, A. T. , Leichti, R. L. , Gartner, B. L., Johnson, G. R. (2005) Effect of growth ring orientation and placement of earlywood and latewood on MOE and MOR of very-small clear Douglas fir. *Wood and FIber Science*, 37(2):207–212.

Hashin, Z. (1969) Theory of Composite Materials, in *Mechanics of Composite Materials*, Pregamon Press, 201–242.

Hoffmeyer, P., Damkilde, L., Pedersen, T. N. (2000) Structural timber and glulam in compression perpendicular to grain. *Holz als Roh - und Werkstoff*, 58:73–80.

Jernkvist L., Thuvander, F. (2001) Experimental determination of stiffness variation across growth rings in *Picea abies. Holzforschung*, 55(3):309–317.

Jones, R. M. (1975) Mechanics of Composite Materials. McGraw-Hill, New York.

Kennedy, R. W. (1968) Wood in transverse compression. *Forest Prod. J.*, 18:36–40.

Modén, C. S., Berglund, L. A. (2006) Elastic deformation mechanisms of softwoods in radial tension — cell wall bending or stretching? *Holzforschung*, in press.

Nairn. J. A. (2006) Source code and documentation for NairnFEA FEA software and for NairnFEAMPM visualization software. http://oregonstate.edu/~nairnj/.

Pang, S., Orchard, R., McConchie, D. (1999) Tangential shrinkage of *Pinus Radiata* earlywood and latewood, and its implication for within-ring internal checking. *New Zealand Journal of Forestry Science*, 29(3):484–491.

Price, A. T. (1929) A mathematical discussion on the structure of wood in relation to its elastic properties. *Philosophical Transactions of the Royal Society of London. Series A*, 228:1–62.

Schniewind, A. P. (1959) Transverse anisotropy of wood, *Forest Prod. J.*, 9(10):350-359.

Shipsha, A., Berglund, L. A. (2006) Shear coupling effect on stress and strain distributions in wood subjected to transverse compression. *Composites Science and Technology*, in press.

Taylor, A. M., Gartner, B. L., Morrell, J. J. (2003) Co-incident variations in growth rate and heartwood extractive concentration in Douglas-fir. *Forest Ecology and Management*, 186:257–260.